

# Photogalvanic Effects in Surface States of Topological Insulators under Perpendicular Magnetic Fields

Haoyu Li,<sup>1,2</sup> Kainan Chang,<sup>1,\*</sup> Wang-Kong Tse,<sup>3,†</sup> and Jin Luo Cheng<sup>1,2,‡</sup>

<sup>1</sup>*GPL Photonics Laboratory, State Key Laboratory*

*of Luminescence Science and Technology,*

*Changchun Institute of Optics, Fine Mechanics and Physics,*

*Chinese Academy of Sciences, Changchun 130033, China.*

<sup>2</sup>*University of Chinese Academy of Science, Beijing 100039, China.*

<sup>3</sup>*Department of Physics and Astronomy,*

*The University of Alabama, Alabama 35487, USA.*

(Dated: February 16, 2026)

## Abstract

We present a theoretical study of the nonlinear magneto-optical shift conductivity in the surface states of the prototypical topological insulator  $\text{Bi}_2\text{Se}_3$  under a perpendicular quantizing magnetic field. By describing the electronic states as Landau levels and using a perturbative approach, we derive the microscopic expression for the shift conductivity  $\sigma^{(2);\alpha\beta\gamma}(-\omega, \omega)$ , where  $\alpha, \beta, \gamma = \pm$  stand for the circular polarization of light and  $\omega$  is the light frequency; the spectra are further decomposed into contributions from the interband and intraband optical transitions, for which the selection rules are identified. Considering that the system possesses  $C_3$  point group of symmetry, the nonzero components of the conductivity tensor are  $\sigma^{(2);-++} = [\sigma^{(2);+--}]^*$ . Therefore, a pure circularly polarized light generates zero shift current. In the clean limit, the conductivities are nonzero only for discrete photon energies because of the discrete Landau levels and energy conservation, and they become Lorentzian lineshapes with the inclusion of damping, which relaxes the condition of energy conservation. The dependence of the spectra on the damping parameters, the magnetic fields, and the chemical potentials is investigated in detail. Our results reveal that the shift current is highly tunable by the chemical potential and the magnetic field. These results underscore the potential of topological insulators for tunable, strong nonlinear magneto-optical applications.

PACS numbers: 42.65.-k, 73.20.At, 71.70.Di

Keywords: shift current, topological insulator, surface states, Landau level, selection rules, nonlinear magneto-optical effect

## I. INTRODUCTION

Three-dimensional topological insulators (TIs), known for their insulating bulk and conductive surface states, have attracted considerable interest due to their unique properties, such as spin-momentum locking and strong spin-orbit coupling [1–3]. These features make TIs promising candidates for applications in optoelectronics, spintronics, and quantum computing. In particular, the nonlinear optical response of TIs has been extensively studied both theoretically and experimentally on second-harmonic generation [4–6], third-harmonic gen-

---

\* knchang@ciomp.ac.cn

† wktse@ua.edu

‡ jlcheng@ciomp.ac.cn

eration [7], high-harmonic generation [8, 9], and photogalvanic effects [10]. Among various nonlinear optical phenomena, the photogalvanic effect – which generates a direct current under uniform illumination – is of significant interest for applications in photodetection and solar energy conversion to surpass the Shockley-Queisser limit [11–13]. A prominent mechanism underlying this effect is the shift current, a second-order bulk photovoltaic effect originating from a real-space charge displacement of electron wavepackets during interband optical transitions [14, 15]. However, the bulk electronic states in TIs are centrosymmetric, and no shift current can be generated; instead, shift currents have been observed on TI surfaces [16], where the inversion symmetry is broken [17]. Theoretical studies have shown the tunability of the shift current by applying strains [18], chemical potential [19], and the nanostructures of TI like nanowires [20, 21]. Experimentally, asymmetric carrier distributions around the interface can lead to resonant shift currents, which is confirmed by the time- and angle-resolved photoemission spectroscopy [10], highlighting the role of surface-state topology.

In addition, external magnetic fields provide an extra means to control photocurrent generation [15]. For instance, in  $\text{Bi}_2\text{Se}_3$ , an in-plane magnetic field has been shown to induce a photogalvanic current through the interplay between orbital and Zeeman couplings [17]. However, studies so far have primarily focused on in-plane field configurations, where the formation of Landau levels is suppressed. In contrast, our recent study shows that a strong perpendicular magnetic field – which quantizes the electronic states into discrete Landau levels – can have significant effects on second harmonic generation [22, 23]; thus it is interesting to examine how the shift current can be affected by the quantizing Landau levels, which is the focus of this work. Furthermore, considering that the shift current response requires real absorption of a photon to conserve the energy while second harmonic generation does not, it is also interesting to understand how the discrete Landau levels participate in the photogalvanic effects.

In this work, we address above gaps by presenting a comprehensive theoretical study on the shift conductivity for the surface states of  $\text{Bi}_2\text{Se}_3$  under a perpendicular magnetic field. From this, we derive an explicit expression for the second-order shift conductivity tensor  $\sigma^{(2);\tau\alpha\beta}(-\omega, \omega)$  for circularly polarized light. We show that the shift conductivity can be understood in terms of optical transitions between Landau levels, governed by specific selection rules. The dependence of the shift current on the chemical potential and magnetic

field strength is investigated, providing insight into the tunability of nonlinear magneto-optical responses in topological surface states.

This paper is organized as follows: In Sec. II we present the theoretical model and the shift conductivity expression; in Sec. III we analyze the selection rules, and then discuss results in different chemical potentials and magnetic fields; finally, we conclude in Sec. IV.

## II. MODEL

We study the optical response of the surface states for a topological insulator  $\text{Bi}_2\text{Se}_3$  with applying an external magnetic field  $B$  along the  $z$ -direction. Without the magnetic field, the Hamiltonian is  $H(\mathbf{p}) = v_F(p_y\sigma_x - p_x\sigma_y) + \frac{\lambda}{2\hbar^3}(p_+^3 + p_-^3)\sigma_z$ , where  $v_F$  is the Fermi velocity,  $\mathbf{p}$  is the momentum operator with  $p_{\pm} = p_x \pm ip_y$ ,  $\sigma_{x,y,z}$  are Pauli matrices, and the second term describes the hexagonal warping effects with a strength parameter  $\lambda$  [6, 24]; with the magnetic field, the Hamiltonian becomes  $H(\mathbf{p} + |e|\mathbf{A}) + \Delta\sigma_z$ , where  $\mathbf{A} = (0, Bx, 0)$  gives the vector potential and  $\Delta = g\mu_BB/2$  determines the Zeeman coupling strength [22]. The electronic states and Berry connections have been well studied in our previous work [22], which are briefly summarized as follows: First, the electronic states can be described by Landau levels  $\Psi_s(\mathbf{r})$  with the Landau index  $s = \dots, -2, -1, 0, 1, 2 \dots$ , and the corresponding eigenenergy is  $\varepsilon_s$ . Second, the Berry connection between different Landau levels  $s_1$  and  $s_2$  is  $\xi_{s_1s_2}$ . For a circularly polarized incident light with a polarization vector  $\hat{\mathbf{e}}^{\alpha} = (\hat{\mathbf{x}} + i\alpha\hat{\mathbf{y}})/\sqrt{2}$  with  $\alpha = \pm$ , the light-matter interaction is determined by  $\xi_{s_1s_2}^{\alpha} = \xi_{s_1s_2} \cdot \hat{\mathbf{e}}^{\alpha}$ , where  $\xi_{s_1s_2}^{\alpha}$  is a pure imaginary number and satisfies  $\xi_{s_1s_2}^+ = [\xi_{s_2s_1}^-]^*$ . Without the warping term, and the eigenenergy can be given by  $\varepsilon_s(0) = g_s\sqrt{\Delta^2 + |s|(\hbar\omega_c)^2}$  with  $g_s = \text{sgn}(s)$  for  $s \neq 0$  and  $g_0 = -1$ , and the cyclotron energy  $\hbar\omega_c = \sqrt{2\hbar eBv_F}$ ; the selection rule for  $\xi_{s_1s_2}^+$  is  $|s_1| = |s_2| + 1$ . With the warping term, the correction to the eigenenergy is quite small when the Landau energies are less than bulk gap of  $\text{Bi}_2\text{Se}_3$   $\Delta_{\text{gap}} \approx 300$  meV; and the selection rule for the Berry connections becomes  $|s_1| - |s_2| = 3l + 1$  for any integer  $l$  and its value satisfies  $|\xi_{s_1s_2}^+| \propto \lambda^{|l|}$ ; up to the linear order of the warping term, the values of  $l$  are taken as  $l = 0, \pm 1$ . While such selection rules could in principle be obtained from symmetry arguments, the complexity – introduced by the presence of warping term and the choice of Landau gauge – makes the wavefunctions difficult to handle within a purely symmetry-based analysis. Therefore, we adopt the more direct perturbation

theory; see Ref. 22 for a detailed derivation. Figure 1 (a) illustrates the Landau levels and the allowed optical transitions for  $\xi_{s_1 s_2}^+$ . The underlying particle-hole symmetry is broken, which is crucial for the allowed second-order nonlinear optical response.

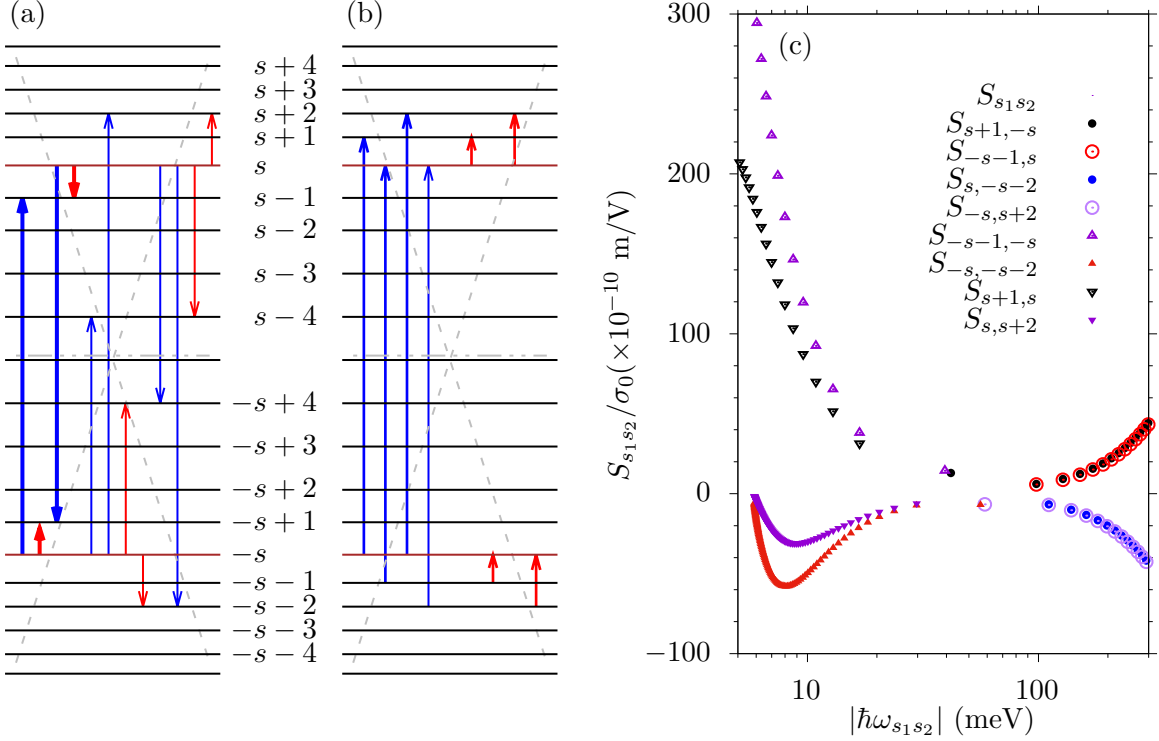


FIG. 1. (a) Illustration of the selection rules for Berry connection  $\xi_{s_1 s_2}^+$  with  $|s_1| - |s_2| = 3l + 1$ , where thick (thin) arrows correspond  $l = 0$  ( $l = \pm 1$ ) with large (small) values. See details in Ref. 22. (b) Illustration of the selection rules for coefficient  $S_{s_1 s_2}$  in shift conductivity with  $|s_1| - |s_2| = 1, -2$ , which is defined in Eq.(5). Note, both in (a) and (b), the blue and red arrows represent interband and intraband transitions, respectively. (c) All nonzero  $S_{s_1 s_2}$  versus their respective discrete transition energies  $|\hbar \omega_{s_1 s_2}|$ , where the Landau energies are calculated at  $B = 5$  T.  $\sigma_0 = e^2/(4\hbar)$ .

In this work, we focus on the direct charge currents generated by a light pulse centered at a frequency  $\omega$ , for which the electric field is  $\mathbf{E}(t) = \mathbf{E}_0(t)e^{-i\omega t} + c.c.$  with the envelope function  $\mathbf{E}_0(t)$  slowly varying with time. Up to the second order of the electric field, the direct current density  $\mathbf{J}(t)$  can be written as  $\mathbf{J}(t) = \sum_{\alpha=\pm} J^\alpha(t) \hat{\mathbf{e}}^\alpha$  with

$$J^\alpha(t) = 2 \sum_{\beta, \gamma=\pm} \sigma^{(2); \alpha\beta\gamma}(-\omega, \omega) \left[ E_0^\beta(t) \right]^* E_0^\gamma(t), \quad (1)$$

where  $\bar{\alpha} = \mp$  for  $\alpha = \pm$  ( $\bar{\beta} = \mp$  for  $\beta = \pm$ ),  $J^\alpha(t) = \mathbf{J}(t) \cdot \hat{\mathbf{e}}^{\bar{\alpha}}$ ,  $E_0^\alpha(t) = \mathbf{E}_0(t) \cdot \hat{\mathbf{e}}^{\bar{\alpha}}$ , and  $\sigma^{(2);\alpha\beta\gamma}(\omega, -\omega)$  the shift conductivity. The microscopic expression of  $\sigma^{(2);\alpha\beta\gamma}(\omega, -\omega)$  is given [22] by  $\sigma^{(2);\alpha\beta\gamma}(\omega, -\omega) = \frac{1}{2} [\tilde{\sigma}^{(2);\alpha\beta\gamma}(\omega, -\omega) + \tilde{\sigma}^{(2);\alpha\gamma\beta}(-\omega, \omega)]$  with

$$\tilde{\sigma}^{(2);\tau\alpha\beta}(-\omega, \omega) = \frac{ie^4 B}{4\pi\hbar^2} \sum_{s_1 s_2 s} \frac{\hbar\omega_{s_1 s_2} \xi_{s_2 s_1}^{\bar{\tau}}}{-\hbar\omega_{s_1 s_2} + i\Gamma_2} \left( \frac{\xi_{s_1 s}^{\alpha} \xi_{s s_2}^{\beta} f_{s_2 s}}{\hbar\omega - \hbar\omega_{s s_2} + i\Gamma_1} - \frac{\xi_{s_1 s}^{\beta} \xi_{s s_2}^{\alpha} f_{s_2 s_1}}{\hbar\omega - \hbar\omega_{s_1 s} + i\Gamma_1} \right). \quad (2)$$

Here  $\hbar\omega_{s_1 s_2} = \varepsilon_{s_1} - \varepsilon_{s_2}$ ,  $f_{s_1 s_2} = f_{s_1} - f_{s_2}$  is the population difference where  $f_s = \theta(\mu - \varepsilon_s)$  is the Fermi-Dirac distribution for a chemical potential  $\mu$  at zero temperature, and  $\Gamma_{1,2}$  are the relaxation parameters.

The surface states of  $\text{Bi}_2\text{Se}_3$  under a magnetic field  $B$  possess symmetry of  $C_3$  point group, which determines the nonzero components of second order tensor  $\sigma^{(2);\tau\alpha\beta}(-\omega, \omega)$  as  $\sigma^{(2);+--}(-\omega, \omega)$  and  $\sigma^{(2);-++}(-\omega, \omega)$  (see Appendix A for symmetry analysis). Furthermore, because  $\mathbf{J}(t)$  is a real number, these two components also satisfy  $\sigma^{(2);-++}(-\omega, \omega) = [\sigma^{(2);+--}(\omega, -\omega)]^* = [\sigma^{(2);+--}(-\omega, \omega)]^*$ , then the dc current is

$$\begin{aligned} \mathbf{J}(t) &= 2\text{Re} [\sigma^{(2);-++}(-\omega, \omega) \hat{\mathbf{e}}^- (E_0^-(t))^* E_0^+(t)] \\ &= \frac{|E_0(t)|^2}{\sqrt{2}} \left[ \cos 2\theta \begin{pmatrix} \sigma_r(\omega) \\ \sigma_i(\omega) \end{pmatrix} + \cos \varphi \sin 2\theta \begin{pmatrix} \sigma_i(\omega) \\ -\sigma_r(\omega) \end{pmatrix} \right]. \end{aligned} \quad (3)$$

Here we note  $\mathbf{E}_0(t) = E_0(t)(\hat{\mathbf{x}} \cos \theta + \hat{\mathbf{y}} \sin \theta e^{i\varphi})$  with two parameters  $\theta$  and  $\varphi$  describing its polarization,  $\sigma_r(\omega) = \text{Re} [\sigma^{(2);-++}(-\omega, \omega)]$  and  $\sigma_i(\omega) = \text{Im} [\sigma^{(2);-++}(-\omega, \omega)]$ . It is easy to find that a pure circularly polarized light ( $\theta = \pi/4$  and  $\varphi = \pm\pi/2$ ) cannot generate shift currents.

### III. RESULTS

#### A. Selection rules

To better understand the direct current response, we rewrite  $\sigma^{(2);-++}(-\omega, \omega)$  as

$$\sigma^{(2);-++}(-\omega, \omega) = \sum_{s_1 s_2} [\mathcal{A}_{s_1 s_2} L_1(\hbar\omega - \hbar\omega_{s_1 s_2}) + i\mathcal{B}_{s_1 s_2} L_2(\hbar\omega - \hbar\omega_{s_1 s_2})] f_{s_2 s_1}, \quad (4)$$

where the coefficients are  $\mathcal{A}_{s_1 s_2} = S_{s_2 s_1} - S_{s_1 s_2}$  and  $\mathcal{B}_{s_1 s_2} = S_{s_1 s_2} + S_{s_2 s_1}$  with

$$S_{s_1 s_2} = \frac{ie^4 B}{4\pi\hbar^2} \sum_s \xi_{s_2 s}^+ \xi_{s s_1}^+ \xi_{s_1 s_2}^+ \left( \frac{1}{\hbar\omega_{s_2 s} + i\Gamma_2} - \frac{1}{\hbar\omega_{s s_1} + i\Gamma_2} \right), \quad (5)$$

and two spectral functions

$$L_1(w) = \frac{\Gamma_1^2}{w^2 + \Gamma_1^2}, \quad L_2(w) = \frac{w\Gamma_1}{w^2 + \Gamma_1^2}. \quad (6)$$

From Eq. (4), the shift conductivity comprises the contributions from transitions between Landau level pairs  $(s_1, s_2)$ . Each contribution is determined by two spectral functions,  $L_1(\hbar\omega - \hbar\omega_{s_1s_2})$  with amplitude  $\mathcal{A}_{s_1s_2}$  and  $L_2(\hbar\omega - \hbar\omega_{s_1s_2})$  with amplitude  $\mathcal{B}_{s_1s_2}$ , both centered at  $\hbar\omega = \hbar\omega_{s_1s_2}$ ; the Pauli blocking factor  $f_{s_2s_1}$  is used to turn on/off the transition between the Landau level pair  $(s_1, s_2)$  by adjusting the chemical potential, *i.e.*, the electron density. In the following, we give a detailed analysis on Eq. (4):

1. We first discuss the selection rules of  $\mathcal{A}$  and  $\mathcal{B}$  by following Ref. 22. The selection rule for  $S_{s_1s_2}$  should satisfy  $|s_1| - |s_2| = 3l_1 + 1$ ,  $|s_2| - |s| = 3l_2 + 1$ , and  $|s| - |s_1| = 3l_3 + 1$  simultaneously for integers  $l_{1,2,3}$ ; thus  $l_1 + l_2 + l_3 = -1$ . It can be found that the leading order of  $S_{s_1s_2}$  is  $\propto \lambda$ , for which  $l_1$  can only take value of 0 or  $-1$ , then the selection rule for  $S_{s_1s_2}$  becomes  $|s_1| - |s_2| = 1$  or  $-2$ . This implies that contributions from  $|s_1| - |s_2| = 4$  transitions are of higher order in  $\lambda$ , making them negligible within the present treatment. Further the selection rules for  $\mathcal{A}_{s_1s_2}$  and  $\mathcal{B}_{s_1s_2}$  are  $|s_1| - |s_2| = \pm 1, \pm 2$ . Note that the selection rules are different from the selection rules for second harmonic generation (SHG) process of Landau levels. By taking the Landau levels  $s \leq 0$  with  $\varepsilon_s < 0$  ( $s > 0$  with  $\varepsilon_s > 0$ ) as valence (conduction) states, all transitions of  $\mathcal{A}_{s_1s_2}$  and  $\mathcal{B}_{s_1s_2}$  can be classified into the interband transitions, which occur between the conduction and valence bands, and intraband transitions, which occur within the conduction or valence bands. All nonzero transitions with positive transition energies are listed in Table I and shown in Fig.1 (b), and the nonzero values of  $S_{s_1s_2}$  are plotted in Fig.1 (c).
2. Because the values of the Berry connections  $\xi_{s_1s_2}^+$  are pure imaginary, thus  $S_{s_1s_2}$  is approximately real for small relaxation parameter  $\Gamma_2$ , further both  $\mathcal{A}_{s_1s_2}$  and  $\mathcal{B}_{s_1s_2}$  are approximately real; then the term involving  $\mathcal{A}$  ( $\mathcal{B}$ ) in Eq. (4) determines the real (imaginary) part of  $\sigma^{(2);-++}$ , which shows two types of spectral functions of  $L_1(\hbar\omega - \hbar\omega_{s_1s_2})$  and  $L_2(\hbar\omega - \hbar\omega_{s_1s_2})$  centered at photon energy  $\hbar\omega_{s_1s_2}$ . In the clean limit as  $\Gamma_1 \rightarrow 0$ , the function  $L_1(\hbar\omega - \hbar\omega_{s_1s_2})$  is nonzero with values of 1 only at  $\hbar\omega - \hbar\omega_{s_1s_2}$ , which reflects the energy conservation. However, this behavior is totally different from

that in the usual shift current in a crystal, where the energy conservation lies in the Dirac-delta function  $\delta(\hbar\omega - \hbar\omega_{s_1s_2})$ ; such a difference is induced by the discreteness of the Landau levels. It is also different from the SHG in Landau levels, where a Dirac-delta function [22] also exists and the conductivity diverges as the photon energy approaches the transition energy in the clean limit; such a difference indicates the fundamentally distinct physical processes underlying the shift current and SHG. In this case,  $L_2 = 0$ , thus the shift current response exists only for discrete photon energies. For finite  $\Gamma_1$ ,  $L_1$  shows a Lorentzian type lineshape with a maximum 1 located at  $\hbar\omega = \hbar\omega_{s_1s_2}$ ; while the spectral shape  $L_2$  shows two extremes with values of  $\pm\frac{1}{2}$  located at  $\hbar\omega = \hbar\omega_{s_1s_2} \pm \Gamma_1$ , and  $L_2(\hbar\omega - \hbar\omega_{s_1s_2})$  is always zero for  $\hbar\omega = \hbar\omega_{s_1s_2}$ . Therefore, when the photon energy matches the transition energy,  $\sigma^{(2);-++}$  becomes purely real with  $\sigma_i(\omega = \omega_{s_1s_2}) = 0$ . Consequently, the shift current in Eq. (3) simplifies to

$$\mathbf{J}(t) = \frac{|E_0(t)|^2}{\sqrt{2}} \sigma_r(\omega_{s_1s_2}) \begin{pmatrix} \cos 2\theta \\ \cos \phi \sin 2\theta \end{pmatrix}, \quad (7)$$

and its direction shows a definite relation with the light polarization.

3. For a small warping parameter,  $\varepsilon_s \approx -\varepsilon_{-s}$  for  $s \geq 1$ ; some transitions have the same transition energies (they are called as “degenerate transitions”). For example, the transitions of  $\mathcal{A}_{s+2,-s}$  and  $\mathcal{A}_{s,-s-2}$  are degenerate transitions. However, they can be turned on/off independently by adjusting the chemical potential  $\mu$ . By defining  $\mu_j$  as the chemical potential for which the highest occupied Landau level is  $j$ ,  $\mathcal{A}_{s+2,-s}$  is allowed only when the Fermi level is at  $\mu_j$  with  $j = s$  or  $s + 1$ , whereas  $\mathcal{A}_{s,-s-2}$  is allowed only at  $\mu_j$  with  $j = -s - 2$  or  $-s - 1$ .
4. The population difference  $f_{s_2s_1}$  for  $s_1 > s_2$  is not zero only for  $\mu_j$  with  $s_1 \leq j < s_2$ . A specific transition contributes to the conductivity only at some filling factors:  $\mathcal{A}_{1,0}$  only contributes at  $\mu_0$ , while  $\mathcal{A}_{2,0}$  can contribute at both  $\mu_0$  and  $\mu_1$ ; similar cases can be found for all intraband transitions. However, some interband transitions can contribute for many chemical potentials. For example, both  $\mathcal{A}_{s+1,-s}$  and  $\mathcal{A}_{s,-s-1}$  contribute for  $\mu_j$  with  $-s \leq j \leq s - 1$ , yielding a combined transition amplitude  $(\mathcal{A}_{s+1,-s} + \mathcal{A}_{s,-s-1})$ , while each additionally contributes at  $\mu_s$  and  $\mu_{-s-1}$ , respectively. All these features are summarized in Table I.

TABLE I. All possible transitions for  $\mathcal{A}_{s_1,s_2}$  and  $\mathcal{B}_{s_1,s_2}$  for  $s_1 > s_2$  with positive transition energies. The column  $X_{s_1s_2}$  stands for  $\mathcal{A}$  or  $\mathcal{B}$  with  $s \geq 1$ ; the column “value” expresses the values of  $X$  as  $S$  with the sign  $(-)$  for  $\mathcal{B}$ ; the column “ $\hbar\omega_{s_1s_2}$ ” is the approximate transition energy for  $X$ , and the column “ $\mu_j$ ” is the filling factor. “DT” means degenerate transitions.

interband transition				intraband transition				
$X_{s_1s_2}$	value	$\hbar\omega_{s_1s_2}$	$\mu_j$	$X_{s_1s_2}$	value	$\hbar\omega_{s_1s_2}$	$\mu_j$	
$X_{1,0}$	$S_{1,0}$	$\varepsilon_1 - \varepsilon_0$	/	0	$X_{0,-2}$	$S_{0,-2}$	$\varepsilon_0 + \varepsilon_2$	
$X_{2,0}$	$(-)S_{0,2}$	$\varepsilon_2 - \varepsilon_0$	/	0, 1	$X_{0,-1}$	$(-)S_{-1,0}$	$\varepsilon_0 + \varepsilon_1$	
DT	$X_{s+1,-s}$	$S_{s+1,-s}$	$\varepsilon_{s+1} + \varepsilon_s$	$[-s, s - 1]$	$s$	$X_{s+1,s}$	$S_{s+1,s}$	$s$
	$X_{s,-s-1}$	$(-)S_{-s-1,s}$			$-s - 1$	$X_{-s,-s-1}$	$(-)S_{-s-1,-s}$	$-\bar{s}$
DT	$X_{s+2,-s}$	$(-)S_{-s,s+2}$	$\varepsilon_{s+2} + \varepsilon_s$	$[-s, s - 1]$	$s,$ $s + 1$	$X_{s+2,s}$	$(-)S_{s,s+2}$	$s,$ $s + 1$
	$X_{s,-s-2}$	$S_{s,-s-2}$			$-s - 2,$ $-s - 1$	$X_{-s,-s-2}$	$S_{-s,-s-2}$	$-\bar{s} - 2,$ $-\bar{s} - 1$

## B. Shift conductivity at $B = 5$ T

Here we take  $v_F = 5 \times 10^5$  m/s,  $\lambda = 165$  eV· Å<sup>3</sup>,  $g = 8.4$ , and  $T = 0$  K [22]. Unless otherwise specified, the relaxation parameters are  $\Gamma_1 = \Gamma_2 = 1.3$  meV.

Figures 2 (a, b) show the real and imaginary parts of the spectra  $\sigma^{(2);-++}$  under a magnetic field  $B = 5$  T and a chemical potential  $\mu = 0$  eV (filling factor  $\mu_0$ ). According to Table I, only interband transitions contribute to the conductivity in this case, namely  $X_{1,0}$ ,  $X_{2,0}$ ,  $X_{s+1,-s} + X_{s,-s-1}$ , and  $X_{s+2,-s} + X_{s,-s-2}$  for  $s \geq 1$ . The spectra of  $\sigma_r(\omega)$  in Fig. 2 (a) exhibit discrete peaks, which are determined by  $\mathcal{A}_{1,0}$ ,  $\mathcal{A}_{2,0}$ ,  $\mathcal{A}_{s+1,-s} + \mathcal{A}_{s,-s-1}$ , and  $\mathcal{A}_{s+2,-s} + \mathcal{A}_{s,-s-2}$  for  $s \geq 1$ , located at the transition energies  $\hbar\omega_{1,0} \sim 41.8$  meV,  $\hbar\omega_{2,0} \sim 58.5$  meV,  $\hbar\omega_{s+1,-s}$ , and  $\hbar\omega_{s+2,-s}$  for  $s \leq 1$ , respectively. It is interesting that the first two peaks are an order of magnitude higher than subsequent ones. This is because the former originate from individual transitions, while the latter are induced by degenerate transitions ( $\mathcal{A}_{s+1,-s}$  and  $\mathcal{A}_{s,-s-1}$ , or  $\mathcal{A}_{s+2,-s}$  and  $\mathcal{A}_{s,-s-2}$  for  $s \geq 1$ ), which have comparable amplitudes but opposite signs, leading to a significant cancellation. The spectra of  $\sigma_i(\omega)$  in Fig. 2 (b) also show discrete lineshapes formed by  $L_2(\hbar\omega - \hbar\omega_{s_1s_2})$ . Different from  $\sigma_r(\omega)$ , the degenerate transitions

$\mathcal{B}_{s+1,-s} + \mathcal{B}_{s,-s-1}$  and  $\mathcal{B}_{s+2,-s} + \mathcal{B}_{s,-s-2}$  do not cancel each other. Therefore, with the photon energy increases, the peak values increase as well.

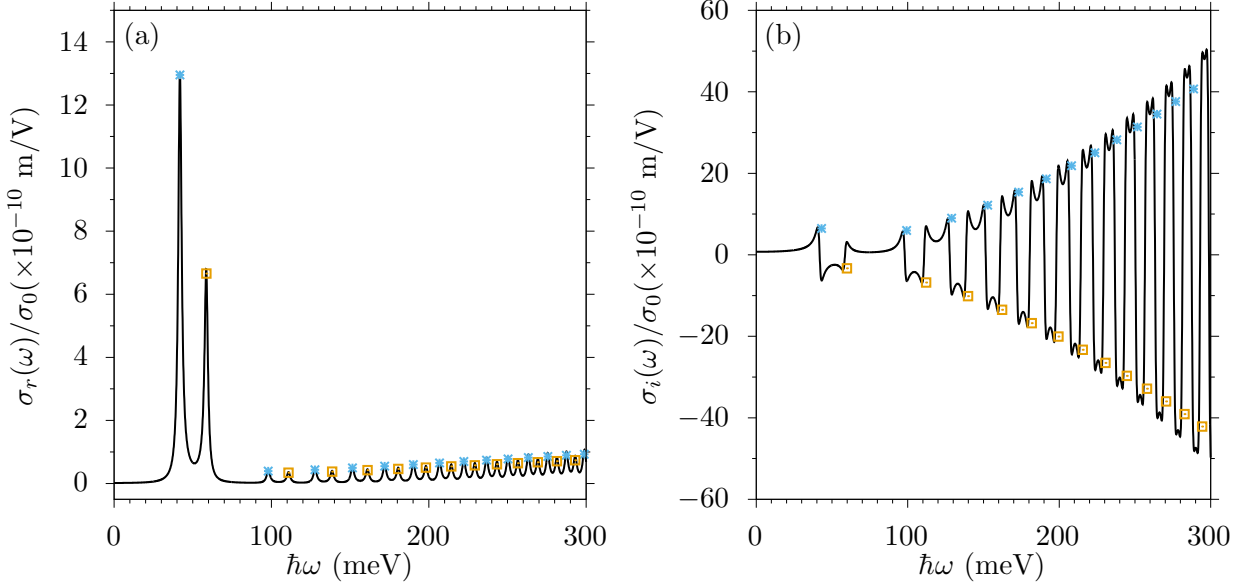


FIG. 2. (a) The spectra of  $\sigma_r(\omega)$  and the values of  $\mathcal{A}_{s_1s_2}$  with  $|s_1| - |s_2| = \pm 1$  (star symbols) and with  $|s_1| - |s_2| = \pm 2$  (square symbols). (b) The spectra of  $\sigma_i(\omega)$  and the values of  $\mathcal{B}_{s_1s_2}$  with  $|s_1| - |s_2| = \pm 1$  (star symbols) and with  $|s_1| - |s_2| = \pm 2$  (square symbols).

### C. Relaxation energy dependence

Figure 3 shows the spectra of the conductivity  $\sigma_{r/i}(\omega)$  for different relaxation parameters  $\Gamma_1 = \Gamma_2 = 0.9, 1.3$ , and  $2 \text{ meV}$ . For  $\sigma_r(\omega)$ , it can be seen that with the increasing  $\Gamma$ , both the peak location and the peak value remain essentially unchanged, but the peak width increases significantly. The peak value hardly changes because the maximal value of  $L_1(w)$  is independent of the relaxation energy. Such relaxation parameter insensitivity indicates that  $\sigma_r(\omega)$  does not include the contribution from the injection current process, and  $\sigma^{(2);-++}(\omega)$  is the shift conductivity. In contrast, for  $\sigma_i(\omega)$ , both the locations and values of these extremes are slightly changed. The shifts of locations are because they depend on  $\Gamma$ , but the changes in the extreme values are induced by  $\Gamma$ -dependent  $\mathcal{A}_{s_1s_2}$ . Notably, the insensitivity of the peak values of the shift current to  $\Gamma$  contrasts with many conventional nonlinear magneto-optical effects (e.g., injection current or SHG) [22, 25, 26], where the

response strength strongly depends on the relaxation parameter. This distinction shows the unique shift current in topological surface states under quantizing magnetic fields.

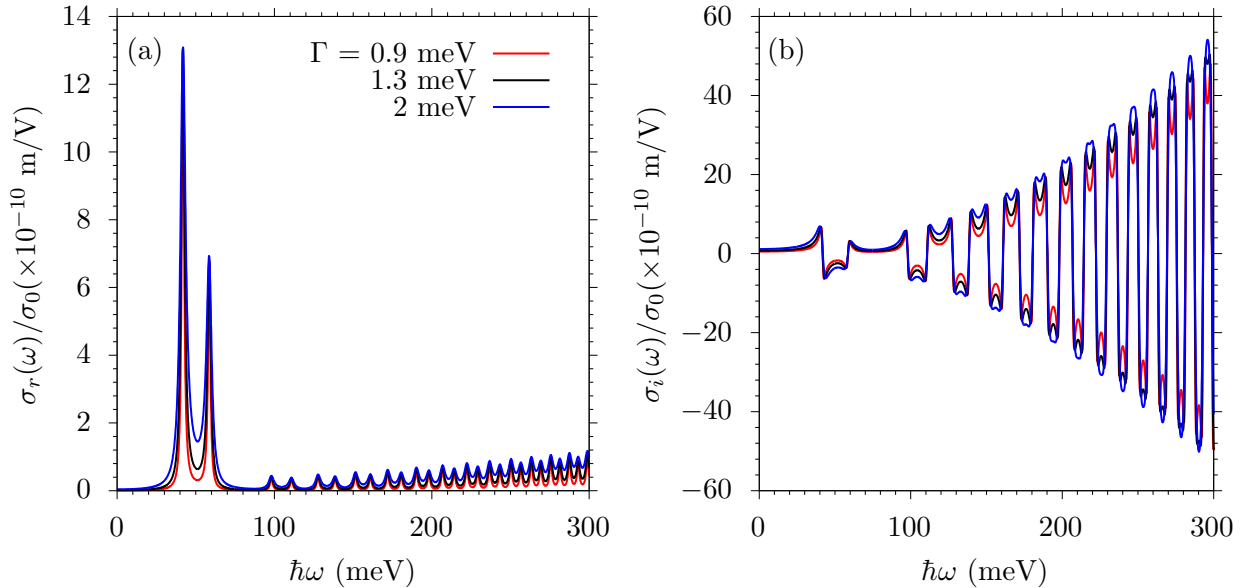


FIG. 3. Spectra of (a)  $\sigma_r(\omega)$  and (b)  $\sigma_i(\omega)$  for different relaxation parameters  $\Gamma$ .

#### D. Chemical potential dependence

Now we study how the shift conductivity is affected by the chemical potential  $\mu$ , or filling factor  $\mu_s$ . As an example, Fig. 4 (a) shows the spectra of  $\sigma_r(\omega)$  for different  $\mu_s$  for  $-2 \leq s \leq 2$ . Compared to the case for  $\mu_0$ , the difference of the spectra at different  $\mu_s$  arises from the Pauli blocking effects: (1) Some of the interband transitions are blocked and the corresponding peaks disappear, and lowest interband transition energy increases for  $\mu_s$  with larger  $|s|$ . Taking  $\mu_2$  as an example, from Table I, all available interband transitions are  $\mathcal{A}_{s+1,-s} + \mathcal{A}_{s,-s-1}$  and  $\mathcal{A}_{s+2,-s} + \mathcal{A}_{s,-s-2}$  for  $s \geq 3$ ,  $\mathcal{A}_{3,-2}$ ,  $\mathcal{A}_{3,-1}$ , and  $\mathcal{A}_{4,-2}$ . The first interband transition starts from larger energy  $\hbar\omega_{3,-1}$ . Compared to the case for  $\mu_0$ , there disappear five interband transitions of  $\mathcal{A}_{1,0}$ ,  $\mathcal{A}_{2,0}$ ,  $\mathcal{A}_{2,-1}$ ,  $\mathcal{A}_{1,-3}$ , and  $\mathcal{A}_{2,-4}$ , where the latter three breaks the degenerate transition and induce relative large peaks located at  $\hbar\omega_{2,-1}$ ,  $\hbar\omega_{1,-3}$ , and  $\hbar\omega_{2,-4}$ . (2) There appears intraband transitions. For  $\mu_2$ , they are  $\mathcal{A}_{3,2}$ ,  $\mathcal{A}_{4,2}$ , and  $\mathcal{A}_{3,1}$ , which correspond to lower transition energies, but with large amplitudes. For  $\mu_s$  with large  $s$ , the first intraband transition energy is  $\hbar\omega_{|s|+1,|s|}$ , which decreases with increasing

$|s|$ . The intraband transition shows analogous to the Drude contribution. Similar analysis can be applied for other  $\mu_s$ . Figure 4 (b, c) show the spectra of  $\sigma_r(\omega)$  and  $\sigma_i(\omega)$  for more  $\mu_s$  with  $-8 \leq s \leq 8$ . For higher doped system, the predominant responses occur in the lower photon energy regime induced by the intraband transitions and in the higher photon energy regime induced by interband transitions; no shift current response exists between these two energy regimes. Schematic diagrams illustrating the allowed and forbidden transitions for  $S_{s_1, s_2}$  are presented in Figs. 4 (d) and (e), where the filling factors are  $\mu_0$  and  $\mu_s$  ( $s > 0$ ), respectively. For  $\mu_0$ , both interband transitions within each degenerate pair are allowed, and no intraband transition occurs. In contrast, for  $\mu_s$ , only one transition in each interband degenerate pair is allowed – the other is Pauli-blocked, and among intraband transitions, only those near to the Fermi level become active.

### E. Magnetic field dependence

Then we turn to the magnetic field dependence of  $\sigma^{(2);-++}$ . Figures 5 (a, b) show the spectra of  $\sigma_r$  and  $\sigma_i$  as functions of  $\hbar\omega/\hbar\omega_c$  for  $\hbar\omega < 300$  meV at  $\mu = 0$  eV under  $B = 0.5$ , 2, and 5 T. From the previous analysis, as the magnetic field increases, the cyclotron energy  $\hbar\omega_c$  increases, and the energy differences between Landau levels also increase; therefore, the peak positions of  $\sigma_{r/i}$  shift to higher energies and the intervals between peaks also increase. With the energy scaling factor  $\hbar\omega_c$ , it is obvious that all peaks and oscillations are located approximately at the same values of  $\hbar\omega/\hbar\omega_c$ . At  $B = 0.5$  T, the peak intervals of  $\sigma_r$  at  $\hbar\omega/\hbar\omega_c > 8.3$  are smaller than the scaled damping parameters  $\Gamma/\hbar\omega_c \sim 0.10$ , and then the neighboring peaks merge into a smooth curve; however,  $\sigma_i$  still show oscillations, although their amplitude is greatly reduced and gradually vanishes at higher photon energies. In fact, with further decreasing the magnetic field to  $B = 0.05$  T,  $\sigma_i$  becomes a smooth curve as well at larger photon energy, as shown in Fig. 5 (c).

To better understand the behavior of the conductivity as the magnetic field goes to zero, we can refer to a symmetry analysis in the limit of  $B = 0$  T, where  $\sigma_r(\omega)$  vanishes [22] but  $\sigma_i(\omega)$  should exist. For small magnetic field, our numerical results show that  $\sigma_r(\omega)$  is proportional to  $B$ , and  $B^{-1}\sigma_r(\omega)$  for  $B = 0.05$  T are shown in Fig. 5 (c) for  $\mu = 0$ , 20, and 40 meV. The spectra show two regions: at the lower photon energies  $B^{-1}\sigma_r(\omega)$  decreases with the photon energy, indicating the intraband contribution to the shift conductivities;

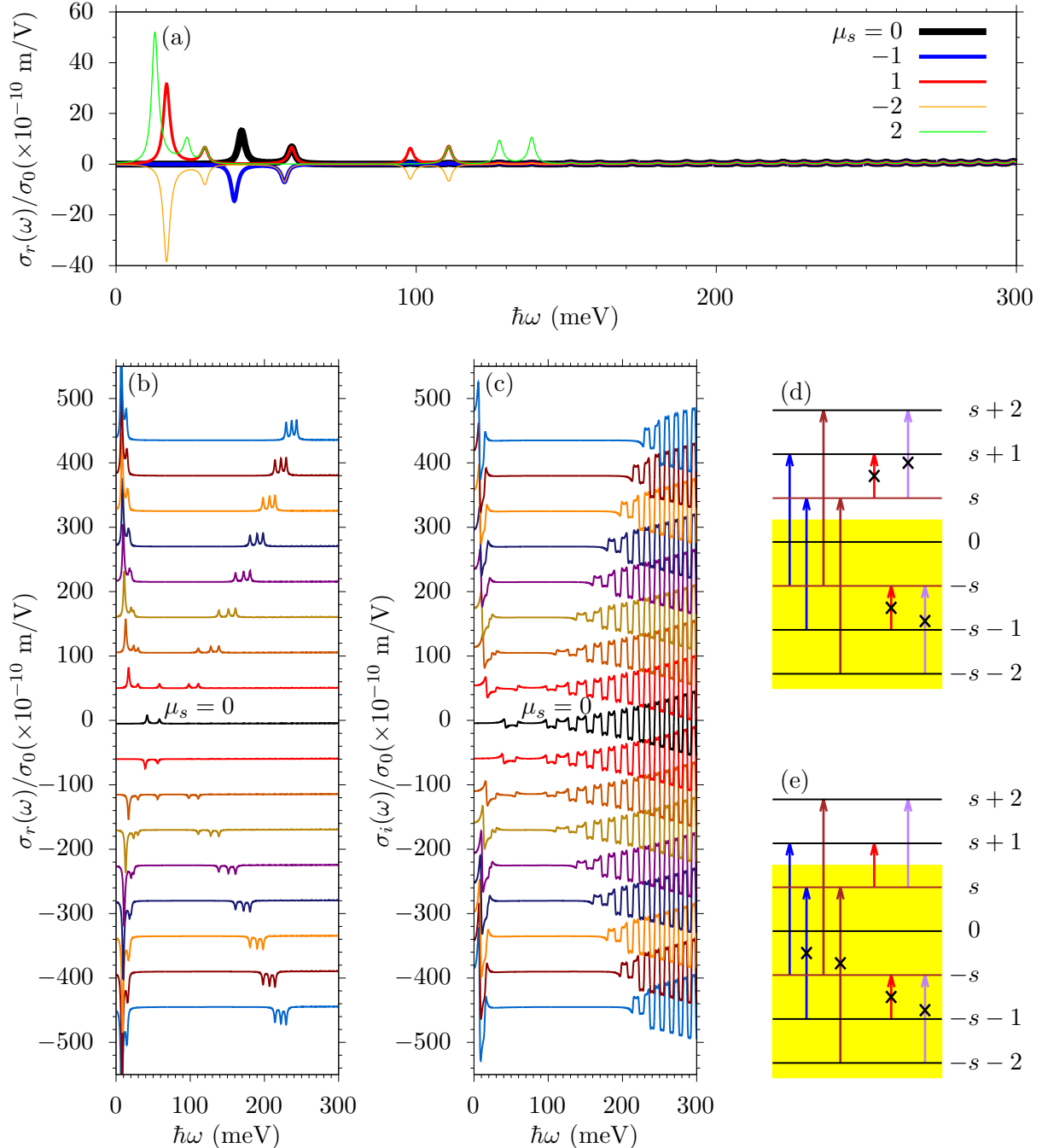


FIG. 4. Shift conductivities with different  $\mu_s$ . (a) displays the spectra of  $\sigma_r(\omega)$  for  $\mu_s = 0, \pm 1, \pm 2$ . (b, c) show the spectra of  $\sigma_r(\omega)$  and  $\sigma_i(\omega)$ , respectively, where the black curve denotes  $\mu_0$ , and other curves above (below) it correspond to increasing (decreasing) values of  $\mu_s$ . Illustration of the selection rules for the coefficient  $S_{s_1s_2}$  when the highest occupied Landau level is (d) 0 and (e)  $s$  with  $s > 0$ , corresponding to the filling factors  $\mu_0$  and  $\mu_s$ , respectively. Arrows of the same color denote a pair of degenerate transitions (see Table I), while crosses mark forbidden transitions.

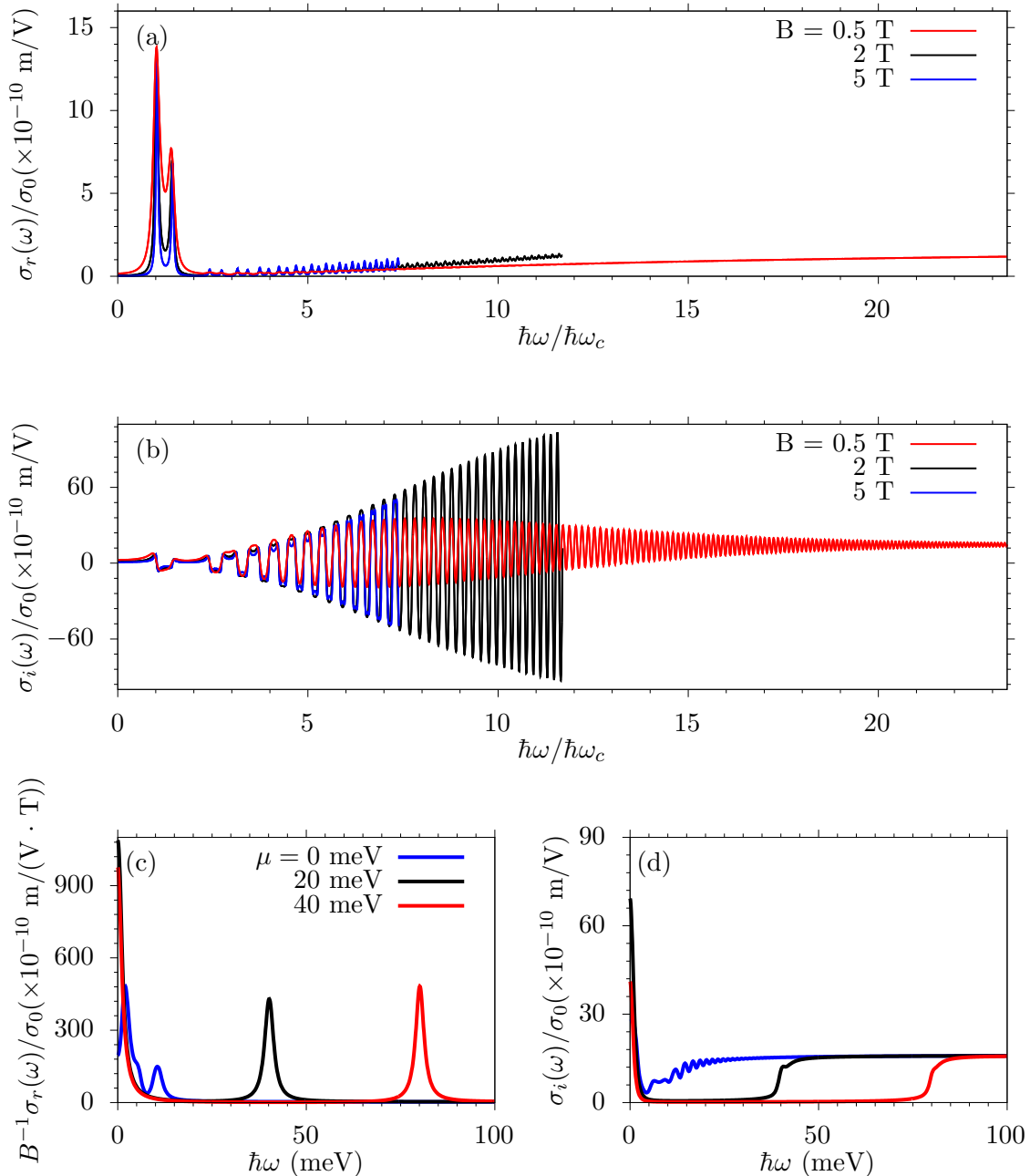


FIG. 5. The spectra of (a)  $\sigma_r(\omega)$  and (b)  $\sigma_i(\omega)$  as functions of  $\hbar\omega/\hbar\omega_c$  for  $\hbar\omega < 300$  meV at  $\mu = 0$  eV and different magnetic field  $B = 0.5, 2$ , and  $5$  T. The spectra of (c)  $B^{-1}\sigma_r(\omega)$  and (d)  $\sigma_i(\omega)$  with different chemical potentials  $\mu = 0, 20$ , and  $40$  meV for  $B = 0.05$  T.

there appears a peak at  $\hbar\omega \approx 2|\mu|$ , indicating the contributions from the interband transitions. At a small magnetic field,  $\sigma_i(\omega)$  is nonzero, and its spectra are also shown in Fig. 5 (c) for chemical potential  $\mu = 0, 20, 40$  meV. The resonant peaks are associated with the

chemical potential  $\mu$ , which is similar with second harmonic generation [22]. At the lower photon energy regime,  $\sigma_i(\omega)$  show similar features as that of  $B^{-1}\sigma_r(\omega)$ , however, the interband contributions approximately show a step function, where the values at  $\hbar\omega > 2|\mu|$  are approximately independent of the photon energy.

#### IV. CONCLUSION

In summary, we have investigated the nonlinear magneto-optical conductivity associated with the shift current in the surface states of the topological insulator  $\text{Bi}_2\text{Se}_3$  under a perpendicular magnetic field. By describing the electronic states as Landau levels and employing a perturbative approach, we derived the microscopic expression for the shift conductivity tensor. It shows that the shift current can be generated when the light is not pure circularly polarized, and exhibit both  $x$  and  $y$  components, which arise from resonant optical transitions between occupied Landau levels  $s_1$  and unoccupied Landau levels  $s_2$ , governed by the selection rules  $|s_1| - |s_2| = \pm 1, \pm 2$ .

We provide a detailed analysis of the contributions from intraband and interband transitions to the conductivity spectra, along with their dependence on damping parameters, chemical potentials, and magnetic fields. Intraband transitions occur at lower transition energies, whereas interband transitions contribute at higher energies. The damping parameters primarily affect the spectral linewidths without significantly altering peak amplitudes. The chemical potential significantly tunes the contributions from intraband and interband transitions: at larger chemical potentials, the spectral features from interband transitions shift to higher photon energies, while those from intraband transitions shift to lower photon energies, thereby leaving a photon energy region with negligible photocurrent response.

The peak positions scale approximately with cyclotron energy  $\hbar\omega_c \propto \sqrt{B}$ , while the peak amplitudes exhibit a more complicated dependence due to the interplay between the magnetic fields and the damping parameters. For large damping parameters or very small magnetic fields, the discrete spectral peaks merge into a smooth curve. Under very small magnetic fields, the  $y$ -component of the current is approximately proportional to the magnetic field, whereas the  $x$ -component forms a smooth curve with a resonant peak occurring at a photon energy roughly twice the chemical potential.

When we take the thickness of the surface states as  $d = \hbar v_F / \Delta_{\text{gap}} \approx 9.4 \text{ \AA}$ , which is

estimated as the depth of the surface wave functions penetrating into the bulk [4], the amplitude of effective bulk shift conductivity  $\sigma(\omega)$  can reach  $326 \mu\text{A}/\text{V}^2$  with  $\hbar\omega \approx 297 \text{ meV}$ ,  $B = 5 \text{ T}$  and  $\mu_s = 0$ . This value is of the same order of magnitude as that reported in GeSe (approximately  $200 \mu\text{A}/\text{V}^2$ ) [27]. It is noteworthy that our predicted conductivity can be significantly enhanced through higher doping levels or the stronger magnetic fields. These findings indicate a relaxation dependent insensitive and highly tunable nonlinear magneto-optical response in topological insulators, and suggest their potential as functional nonlinear materials for developing advanced magneto-optical devices.

## ACKNOWLEDGMENTS

Work in China was supported by National Natural Science Foundation of China Grants No. 12034003 (K.C. and J.L.C.). Work in U.S. was supported by the U.S. Department of Energy, Office of Science, Basic Energy Sciences under Early Career Award No. DE-SC0019326 (W-K.T.).

## Appendix A: Symmetry analysis for circularly polarized conductivity

The effective Hamiltonian for the (111) surface of  $\text{Bi}_2\text{Se}_3$  including hexagonal warping respects the  $C_{3v}$  point group, which contains threefold rotations  $C_3$  about the trigonal axis and vertical mirror planes  $M$  [24, 28, 29]. When a uniform magnetic field is applied along the  $z$ -axis, time-reversal symmetry is broken, and the vertical mirror symmetry with respect to the  $yz$  plane is also broken. Consequently, the point-group symmetry of the surface is reduced to the pure rotational subgroup  $C_3$ , generated by a  $2\pi/3$  rotation

$$R_{2\pi/3} : (x, y) \rightarrow \left( x \cos \frac{2\pi}{3} - y \sin \frac{2\pi}{3}, x \sin \frac{2\pi}{3} + y \cos \frac{2\pi}{3} \right). \quad (\text{A1})$$

We adopt the circular polarization vectors

$$\hat{\mathbf{e}}^+ = \frac{\hat{\mathbf{x}} + i\hat{\mathbf{y}}}{\sqrt{2}}, \quad \hat{\mathbf{e}}^- = \frac{\hat{\mathbf{x}} - i\hat{\mathbf{y}}}{\sqrt{2}}, \quad (\text{A2})$$

which transform under  $R_{2\pi/3}$ , as

$$R_{2\pi/3} \hat{\mathbf{e}}^\pm = e^{\pm i2\pi/3} \hat{\mathbf{e}}^\pm. \quad (\text{A3})$$

The dc photocurrent density generated at second order can be written as Eq.(1). The tensor component  $\sigma^{(2);\alpha\beta\gamma}$  must be invariant under the symmetry operations of the system. Under  $C_3$  rotation, the product of field amplitudes transforms as

$$[E^{\bar{\beta}}]^* E^\gamma \rightarrow e^{i(\beta+\gamma)\frac{2\pi}{3}} [E^{\bar{\beta}}]^* E^\gamma. \quad (\text{A4})$$

For the current  $J^\alpha$  to remain invariant, the total phase factor of the term  $\sigma^{(2);\alpha\beta\gamma}[E^{\bar{\beta}}]^* E^\gamma$  must be unity. It implies

$$e^{-i\alpha\frac{2\pi}{3}} = e^{i(\beta+\gamma)\frac{2\pi}{3}}, \quad (\text{A5})$$

or equivalently

$$\alpha \equiv \beta + \gamma \pmod{3}. \quad (\text{A6})$$

Because  $\alpha, \beta, \gamma = +, -$  (represented numerically as +1 and -1), the only independent non-vanishing components are

$$\sigma^{(2);+--}(-\omega, \omega), \quad \text{and} \quad \sigma^{(2);-++}(-\omega, \omega), \quad (\text{A7})$$

with the relation  $\sigma^{(2);-++}(-\omega, \omega) = [\sigma^{(2);+--}(-\omega, \omega)]^*$ . All other components are identically zero under the  $C_3$  point group.

- [1] Wang Y, Deorani P, Banerjee K, Koirala N, Brahlek M, Oh S and Yang H 2015 *Phys. Rev. Lett.* **114**(25) 257202 URL <https://link.aps.org/doi/10.1103/PhysRevLett.114.257202>
- [2] Fan Y, Upadhyaya P, Kou X, Lang M, Takei S, Wang Z, Tang J, He L, Chang L T, Montazeri M, Yu G, Jiang W, Nie T, Schwartz R N, Tserkovnyak Y and Wang K L 2014 *Nat. Mater.* **13** 699–704 ISSN 1476-1122
- [3] Yazyev O V, Moore J E and Louie S G 2010 *Phys. Rev. Lett.* **105**(26) 266806 URL <https://link.aps.org/doi/10.1103/PhysRevLett.105.266806>
- [4] McIver J W, Hsieh D, Drapcho S G, Torchinsky D H, Gardner D R, Lee Y S and Gedik N 2012 *Phys. Rev. B* **86**(3) 035327 URL <https://link.aps.org/doi/10.1103/PhysRevB.86.035327>
- [5] Glinka Y D, Babakiray S, Johnson T A, Holcomb M B and Lederman D 2015 *Phys. Rev. B* **91**(19) 195307 URL <https://link.aps.org/doi/10.1103/PhysRevB.91.195307>

- [6] Li Z and Nori F 2019 *Phys. Rev. B* **99**(15) 155146 URL <https://link.aps.org/doi/10.1103/PhysRevB.99.155146>
- [7] Giorgianni F, Chiadroni E, Rovere A, Cestelli-Guidi M, Perucchi A, Bellaveglia M, Castellano M, Di Giovenale D, Di Pirro G, Ferrario M, Pompili R, Vaccarezza C, Villa F, Cianchi A, Mostacci A, Petrarca M, Brahlek M, Koirala N, Oh S and Lupi S 2016 *Nat. Commun.* **7** ISSN 2041-1723
- [8] Bai Y, Fei F, Wang S, Li N, Li X, Song F, Li R, Xu Z and Liu P 2021 *Nat. Phys.* **17** 311–315 ISSN 1745-2473
- [9] Baykusheva D, Chacon A, Lu J, Bailey T P, Sobota J A, Soifer H, Kirchmann P S, Rotundu C, Uher C, Heinz T F, Reis D A and Ghimire S 2021 *Nano Lett.* **21** 8970–8978 ISSN 1530-6984
- [10] Soifer H, Gauthier A, Kemper A F, Rotundu C R, Yang S L, Xiong H, Lu D, Hashimoto M, Kirchmann P S, Sobota J A and Shen Z X 2019 *Phys. Rev. Lett.* **122**(16) 167401 URL <https://link.aps.org/doi/10.1103/PhysRevLett.122.167401>
- [11] Zheng Z, Chang K and Cheng J L 2023 *Phys. Rev. B* **108**(23) 235401 URL <https://link.aps.org/doi/10.1103/PhysRevB.108.235401>
- [12] Kaner N T, Wei Y, Jiang Y, Li W, Xu X, Pang K, Li X, Yang J, Jiang Y, Zhang G and Tian W Q 2020 *ACS Omega* **5** 17207–17214 pMID: 32715206 URL <https://doi.org/10.1021/acsomega.0c01319>
- [13] Cook A M, M Fregoso B, de Juan F, Coh S and Moore J E 2017 *Nature Communications* **8** 14176
- [14] Matsuo H and Noguchi Y 2024 *Jpn. J. Appl. Phys.* **63** ISSN 0021-4922
- [15] Dai Z and Rappe A M 2023 *Phys. Rev. B* **107**(20) L201201 URL <https://link.aps.org/doi/10.1103/PhysRevB.107.L201201>
- [16] McIver J W, Hsieh D, Steinberg H, Jarillo-Herrero P and Gedik N 2012 *Nat. Nanotechnol.* **7** 96–100 ISSN 1748-3387
- [17] Junck A, Refael G and von Oppen F 2013 *Phys. Rev. B* **88**(7) 075144 URL <https://link.aps.org/doi/10.1103/PhysRevB.88.075144>
- [18] Yang M and Zhang C 2024 *J. Phys. Chem. C* **128** 13373–13378 ISSN 1932-7447
- [19] Okada K N, Ogawa N, Yoshimi R, Tsukazaki A, Takahashi K S, Kawasaki M and Tokura Y 2016 *Phys. Rev. B* **93**(8) 081403 URL <https://link.aps.org/doi/10.1103/PhysRevB.93.081403>

- [20] Meyer N, Geishendorf K, Walowski J, Thomas A and Muenzenberg M 2020 *Appl. Phys. Lett.* **116** ISSN 0003-6951
- [21] Meyer N, Geishendorf K, Walowski J, Thomas A and Muenzenberg M 2020 *Appl. Phys. Lett.* **117** ISSN 0003-6951
- [22] Chang K, Zubair M, Cheng J L and Tse W K 2025 *Phys. Rev. B* **111**(20) 205408 URL <https://link.aps.org/doi/10.1103/PhysRevB.111.205408>
- [23] Cheng J L and Guo C 2018 *Phys. Rev. B* **97**(12) 125417 URL <https://link.aps.org/doi/10.1103/PhysRevB.97.125417>
- [24] Yar A, Jasra and Sabeeh K 2022 *J. Appl. Phys.* **131** 184401 ISSN 0021-8979 URL <https://doi.org/10.1063/5.0090445>
- [25] Meng F, Walla F, Kovalev S, Deinert J C, Ilyakov I, Chen M, Ponomaryov A, Pavlov S G, Hübers H W, Abrosimov N V, Jungemann C, Roskos H G and Thomson M D 2023 *Phys. Rev. Res.* **5**(4) 043141 URL <https://link.aps.org/doi/10.1103/PhysRevResearch.5.043141>
- [26] Boyd R W 2020 *Nonlinear Optics* 4th ed (Academic)
- [27] Rangel T, Fregoso B M, Mendoza B S, Morimoto T, Moore J E and Neaton J B 2017 *Phys. Rev. Lett.* **119**(6) 067402 URL <https://link.aps.org/doi/10.1103/PhysRevLett.119.067402>
- [28] Fu L 2009 *Phys. Rev. Lett.* **103**(26) 266801 URL <https://link.aps.org/doi/10.1103/PhysRevLett.103.266801>
- [29] Hsieh D, McIver J W, Torchinsky D H, Gardner D R, Lee Y S and Gedik N 2011 *Phys. Rev. Lett.* **106**(5) 057401 URL <https://link.aps.org/doi/10.1103/PhysRevLett.106.057401>